Cement and Concrete Research 40 (2010) 1631–1638

Contents lists available at ScienceDirect

Cement and Concrete Research

journal homepage: http://ees.elsevier.com/CEMCON/default.asp

# Electrohydraulic shock wave generation as a means to increase intrinsic permeability of mortar

O. Maurel [b], T. Reess [a], M. Matallah [c], A. De Ferron [a], W. Chen [b], C. La Borderie [b], G. Pijaudier-Cabot [d,*], A. Jacques [e], F. Rey-Bethbeder [e]

[a] Laboratoire de Génie Electrique, Université de Pau, Hélioparc Pau-Pyrénées, 2 Avenue du Président Angot, 64053 PAU CEDEX 9, France
[b] Laboratoire de Sciences Appliquées au Génie Civil et Côtier (LaSAGEC$^2$), Université de Pau, Allée du Parc Montaury, 64600 Anglet, France
[c] RISAM (RISk Assesment & Management), Université de Tlemcen, BP230, Algérie
[d] Laboratoire des Fluides Complexes, Université de Pau, BP 1155, 64013 Pau Cedex, France
[e] Total, CSTJF, Avenue Larribau, 64018 Pau Cedex, France

ARTICLE INFO

*Article history:*
Received 22 March 2010
Accepted 30 July 2010

*Keywords:*
Microstructure (B)
Microcracking (B)
Permeability (C)
Mortar (E)
Mechanical properties (C)

ABSTRACT

This article discusses the influence of compressive shock waves on the permeability of cementitious materials. Shock waves are generated in water by Pulsed Arc Electrohydraulic Discharges (PAED). The practical aim is to increase the intrinsic permeability of the specimens. The maximum pressure amplitude of the shock wave is 250 MPa. It generates damage in the specimens and the evolution of damage is correlated with the intrinsic permeability of the mortar. A threshold of pressure is observed. From this threshold, the increase of permeability is linear in a semi-log plot. The influence of repeated shocks on permeability is also discussed. Qualitative X Ray Tomography illustrates the evolution of the microstructure of the material leading to the increase of permeability. Comparative results from mercury intrusion porosimetry (MIP) show that the micro-structural damage process starts at the sub-micrometric level and that the characteristic size of pores of growing volume increases.

## 1. Introduction

There is considerable interest in the use of Pulsed Arc Electrohydraulic Discharges (PAED) in engineering practice. They can be used for several purposes, for instance water treatment for the separation of organic chemical impurities, acoustic sources in medical or sonar applications, selective separation of solids, or plasma blasting in the mining industry. Depending on the discharge conditions, the electrical energy is transformed into light, heat or mechanical energy.

In this paper, we consider PAED in water as a mean to generate dynamic shock waves impacting mortar samples and we investigate the evolution of the intrinsic permeability the material. The ultimate purpose of this study is to consider dynamic loads induced by PAED as an alternative to hydraulic fracturing of oil and gas reservoirs. The motivation for using dynamic loads instead of the static loads involved in hydraulic fracturing is that in dynamics, dense micro-cracking is expected to occur in the bulk material surrounding the borehole. Compared to statics where damage localises into a set of macro-cracks, the bulk material permeability would be expected to increase over a reasonably large volume. This would provide a potential efficient way to stimulate gas production from tight reservoirs in which the permeability is so small that gas cannot reach macro-fractures (if the attenuation if the dynamic wave is not too important). Obviously several technological challenges should be faced before reaching such a practical application. We report here preliminary results on a mortar, designed to mimic typical tight rocks that can be found in tight gas reservoirs, subjected to compression waves generated by PAED.

The effect of a static load on the permeability of mortar and concrete has been investigated on many occasions in theoretical and experimental studies [5,9,11], nevertheless the specific role of dynamic loads has never been considered although some differences are expected. First of all, the rate dependent response of the material should require dynamic load levels that are expected to be higher than static load levels in order to produce a significant increase of material permeability due to cracking and damage. Second, and more importantly, micro-cracking should be distributed with an increase of the number of small micro-cracks and less macro-cracks compared to statics [3,4]. In dynamics, damage is therefore expected to be more diffuse, affecting the bulk material, instead of growing in a localised process evolving in a very small volume of material. The specificity of such a dynamic damage (fragmentation) process has been explained e.g. by Denoual and Hild in the case of ceramics with a statistical model [6]. Although damage is expected to be diffuse, damage induced anisotropy should be expected too, same as in statics. It will not be characterised here as the evolution of permeability is measured parallel to the compressive pressure wave only.

---

* Corresponding author.
*E-mail address:* Gilles.Pijaudier-Cabot@univ-pau.fr (G. Pijaudier-Cabot).

0008-8846/$ – see front matter © 2010 Elsevier Ltd. All rights reserved.
doi:10.1016/j.cemconres.2010.07.005

The objective of this experimental study is to investigate the experimental correlation between the evolution of cracking and damage due to a compression shock wave with the intrinsic permeability of the material and with its microstructure characteristics. The wave is generated under water and then it is transmitted to the specimen which is immersed (diameter 100 mm, height 125 mm). The amplitude of the compressive shock wave is prescribed by the amount of energy that is involved in the PAED. Micro-cracking and compression damage due to local extensions induced by the Poisson's effect develops in the course of loading. Single and repeated shocks are considered. Then, the specimens are cut into discs of thickness equal to 50 mm and their permeability to nitrogen is measured. The intrinsic permeability of the specimen is obtained according to the Klinkenberg model [13]. The specimens are scanned with X-ray tomography in order to visualize qualitatively the correlation between the mechanical loads, the microstructure of the material and the permeability. The pore size distribution of the specimens and its evolution with the applied loads are also investigated with the help of Mercury Intrusion Porosimetry (MIP).

The experimental set-up is described in the following section. We recall also the basic relationships needed in order to characterise PAED and the compression shock waves. Experimental results are discussed in Section 3.

## 2. Experimental set-up

### 2.1. Electric pulse generator

Figs. 1 and 2 present the experimental devices used in this study. A point–point electrode system is immersed in a tank of a capacity of 540 L filled with tap water at room temperature. The electrodes are made of two vertical cylindrical tubes of diameter 30 mm. On their lower ends two stainless steel ovoid electrodes are screwed ($R = 15$ mm). The gap between the two electrodes is $D = 10$ mm. The impulse voltage is obtained by charging storage capacitors of constant $C$ in the range of 5.3 to 84.8 μF (Fig. 2). A triggered spark-gap allows the switching of energy up to 100 kJ into the water. The maximum charging voltage of the capacitors is 40 kV. The voltage impulse and the current are monitored with a North Star probe (100 kV–90 MHz) and a Pearson current monitor (50 kA–4 MHz) respectively.

### 2.2. Characterisation of the dynamic shock wave

The generation of shock waves requires the occurrence of dielectric breakdown in water, after which heat and expansion of the plasma channel between the two electrodes produce the dynamic load. Let us first consider the conditions under which the dielectric breakdown may occur.

Fig. 1. Photograph of the experimental device.

Two different ways exist in order to induce dielectric breakdown in the water between the two electrodes [1]: the first one occurs on a sub-microsecond time scale. If a very high electric field (from 200 kV/cm to more than MV/cm) is applied to the water gap, streamer corona would develop. Even if both electronic and thermal mechanisms have been considered in literature, the mechanism of the streamer formation in water is not yet well understood [10,12]. For such a discharge, the propagation velocities are typically in the range of 10 km/s and the switching energies involved are low (a few joules).

The second breakdown mode in water is called subsonic discharges because its expansion speed does not exceed the range of several tens of meters per second. It is this breakdown mode which has been implemented in the present study. This breakdown mechanism involves the dynamic formation of 'bubbles' in which an electron avalanche develops in the vapour phase following the formation of a bubble [17]. These vapour bubbles are formed due to the injection of electric energy into the water which is converted into heat (see Fig. 3). The volume of the bubbles is directly related to this energy and grows with time. The injected energy denoted as $E(t)$ is calculated using the following relationship:

$$E(t) = \frac{1}{2}C.\left(U_M^2 - U(t)^2\right) \quad (1)$$

where $C$ is the constant (capacity) of the storage capacitor, $U_M$ is the maximum applied voltage and $U(t)$ the voltage level. This energy corresponds to the difference between the energy initially stored in the capacitor and the energy remaining at time $t$ when the volume of the bubbles is measured. The gas volume is roughly proportional to the injected energy once an energy threshold related to the nucleation of the bubbles has been exceeded. A characteristic example of the development of a subsonic discharge in water is illustrated in (Fig. 3), showing three frames. These pictures taken at close time intervals show clearly that the discharge propagation is associated with the development from the HV electrode of gas bubbles which grow as they attempt to fill the inter-electrode space.

When the applied time of energy injection into the water gap is long enough, the volume of the bubbles grows until they fill the whole inter-electrode gap and then dielectric breakdown occurs. A dynamic pressure wave is associated to this breakdown [8]. This shock wave is both the result of the abrupt expansion of the plasma channel and its temperature rise (up to $10^4$ K). After, the pressure wave propagates in water.

This wave has been characterised experimentally with the help of a sensor made of a piezoelectric polymer material, polyvinylidene fluoride PVDF, with a high natural frequency of 100 MHz. Fig. 4 shows a typical record of the pressure waveform and its associated frequency spectrum. The sensor was placed at different locations in the water tank (different distances from the electrodes) and the pressure wave was recorded. Empirical relationships defining the shape of the wave and relating the amplitude to the energy and measurement location have been obtained by Touya et al. [17] and are recalled briefly in the following.

In the present experimental conditions, the dynamic pressures generated by subsonic water discharges have a bi-exponential form approximately. They are characterized by a rise time of about 500 ns and a duration of a few microseconds. The associated frequency spectrum reaches 300 kHz at −20 dB. The general form of the applied pressure pulse is approximated by Eq. (2):

$$P(t) = P_0\left[e^{-at} - e^{-bt}\right] \quad (2)$$

where $P$ is the pressure at time $t$, $P_0$ denotes the peak pressure value and $a$ and $b$ are constants which depend on the experimental

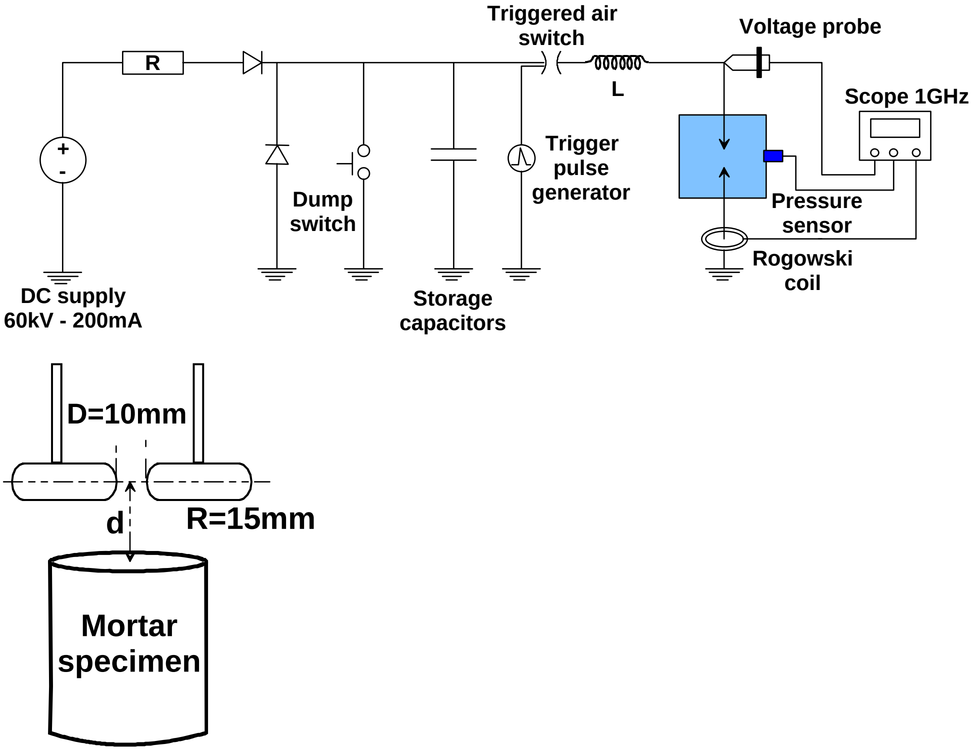

**Fig. 2.** Experimental set up: electrical part (top) and position of the specimen with respect to the electrodes (bottom).

conditions. Results from Touya et al. [17] have pointed out that the peak pressure $P_0$ depends on the energy $E_B$ remaining at breakdown time approximated by the empirical relationship in Eq. (3):

$$P_0 = k.(E_B)^{\alpha} \tag{3}$$

where $E_B = 1/2.C.U_B^2$ ($U_B$ is the breakdown voltage value), $k$ and $\alpha$ are parameters which depend on the inter-electrode geometry and the distance $d$ between the pressure sensor and the plasma channel. In the present experimental geometry ($D = 10$ mm, $R = 15$ mm), $\alpha = 0.35$ and $k = 9000/d$ [17]. Thus, it is possible to obtain an expression of the peak pressure value $P_0$ applied to mortar specimens:

$$P_0 = \frac{9000}{d} \cdot\cdot (E_B)^{0.35} \tag{4}$$

where $P_0$ is given in bar, $E_B$ in kJ and $d$ in mm. The distance between the plasma channel and the surface of the mortar sample denoted as $d$ is varied from 30 mm to 190 mm. During the experiments, the applied peak pressure characterises the pressure wave on the mortar specimens. It is adjusted to the desired value by modifying the distance $d$ (Fig. 2) or by adjusting the value of the electrical energy (Fig. 5).

Due to the configuration of the test set-up, the shock wave is almost spherical and propagates in all the directions in water. It is reflected on the inner surfaces of the water tank and on the surfaces of the mortar cylindrical specimen. A limited part of the energy is converted into a pressure wave applied to the specimen. According to rough calculations based on the propagation of shock waves in water, its reflection/transmission in the specimen, and considering their relative impedance, about 60% of the energy is transmitted to the solid [14]. When the wave is transmitted to the solid, its celerity increases because it is higher in mortar compared to water. Waves reflected on the wall of the tank are thus considered to reach the specimen after the pressure wave which impacted the specimen directly has propagated over the specimen height. Since the size of the water

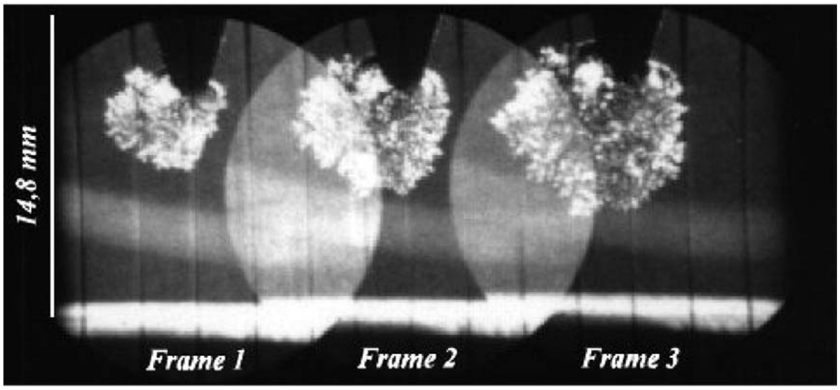

**Fig. 3.** Frames showing bubble development in water [17].

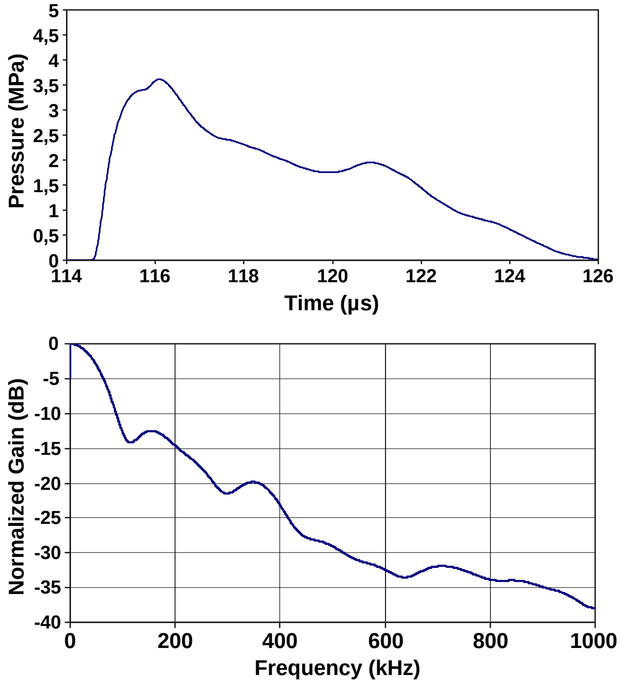

**Fig. 4.** Example of pressure wave (top) and its associated Fourier transform (bottom).

tank is much larger than the size of the specimen; reflected waves which should induce some confinement are not considered to interfere with the damage process in the specimens.

### 2.3. Mortar specimens and their characterisation

An ordinary mortar with a maximal grain size of 2 mm and with a water cement ratio equal to 0.6 has been used. Cylindrical specimens of diameter 100 mm and height 125 mm have been cast in plastic moulds. Half of test specimens were stored in water during 1 month and then kept at a temperature equal to 20 °C and relative humidity equal to 50%. Whereas, the other half was placed during one month in a climatic chamber at fixed temperature (20 °C) and fixed relative humidity (50%). The mean compressive and tensile strengths of this mortar are equal to 19.6 MPa and 4.9 MPa respectively (Table 1). The tensile strength was measured on standardised three point bend specimens (4 × 4 × 16 cm).

The permeability to nitrogen was measured on cylindrical specimens 100 mm diameter and 50 mm height sawed from tested mortars cylinders after mechanical loading and kept in the same environment. The intrinsic permeability of the specimens was obtained according to the Klinkenberg model [13]. The initial permeability of mortar varied between $1 \cdot 10^{-17}$ m$^2$ and $6 \cdot 10^{-17}$ m$^2$. The average value of the initial permeability is considered as a reference in forthcoming results. It characterises the initial state, prior to mechanical loading and micro-cracking. It is important to note that it is the average permeability which is measured here. As the pressure wave propagates inside the specimen, micro-cracking occurs and the micro-crack distribution is not homogeneous over the height of the specimens. As we will see in Section 3.3, micro-cracking is concentrated nearby the surface impacted by the pressure wave. An average variation of permeability corresponding to an average distribution of micro-cracking over a thickness of 50 mm measured from the impacted (top) face of the specimen is obtained.

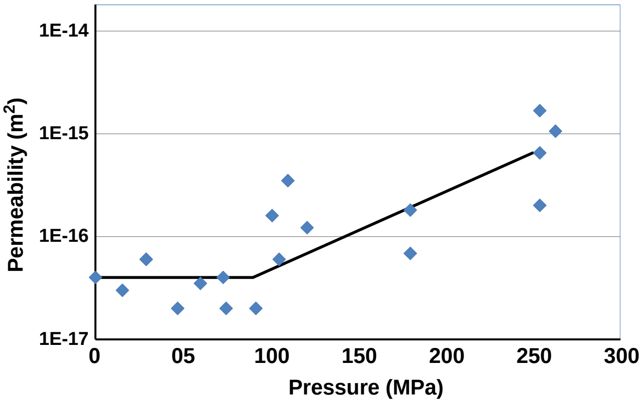

**Fig. 5.** Evolution of the permeability with applied pressure.

**Table 1**
Average mechanical properties of mortar.

| $f_{cm}$ | $f_{tm}$ (MPa) | $E_c$ (MPa) | $K_v$ (m$^2$) |
|---|---|---|---|
| 19.6 | 4.9 | 17 300 | $4.0 \cdot 10^{-17}$ |

In the meantime, the specimens have been scanned with X-ray (micro)-tomography in order to illustrate the correlation between the applied loads, the microstructure of the material and the permeability. The resolution of the scanning device is not very high (250 µm) but differential analyses have been carried out. The specimens were scanned before mechanical testing and after mechanical testing. Then, the two images were subtracted to each other in order to obtain differential measurements of material density. This rather classical image analysis process provided a gain of resolution of two orders of magnitude approximately compared to the resolution of a single scan. Micro-scans of resolution 4 µm were also performed for comparison purposes.

Finally, the pore size distribution was characterised after mechanical testing, according to mercury intrusion porosimetry (MIP). Plugs were drilled from the specimens used for the measurement of permeability (approximately 2 cm$^3$ each) and were oven dried at 80 °C to constant mass. Measurements were repeated on three plugs for each specimen.

## 3. Experimental results

Two sequences of tests have been carried out. In the first one, the specimens have been subjected to a single shock under a variable pressure level. The peak pressure ranged from 0 MPa to 250 MPa (0, 15, 30, 45; 60 90, 180 and 250 MPa). In the second sequence, the specimens have been subjected to repeated shocks at a constant pressure level, equal to 90 MPa. The number of shock waves applied on a single specimen varied from one to ten. Recall that according to simplified dynamic calculations [14], only a limited amount of energy is transmitted to mortar (fraction of roughly 50 to 60% of it).

### 3.1. Influence of peak pressure level on permeability

A single shock is applied on the specimen with amplitude up to 250 MPa. The variation of the intrinsic permeability with the peak pressure is plotted in Fig. 5. Two distinct zones can be observed. If the peak pressure is below 90 MPa, no significant change in permeability is observed. The experimental data in this range span from 2 to $6 \cdot 10^{-17}$ m$^2$ which is a scatter rather usual for the intrinsic permeability of mortar measured on various samples of the same mix. Then, permeability increases almost linearly in a semi-log plot when the peak pressure $P_0$ increases from 90 MPa to 250 MPa. Such a plot, with a threshold above which the permeability grows, is quite typical of the variation of permeability due to a compression stress (see e.g. Refs. [5,15,16]). In a semi-log plot, a linear fit from this pressure describes the permeability increases quite well.

The correlation between the applied loads and the growth of permeability is different in statics and in dynamics however. In statics, the increase of permeability is plotted usually as a function of damage, stress or strain. Here, we have plotted the growth of permeability as a function of the amplitude of the pressure wave which does not generate a homogeneous state of stress, strain or damage. These plots are presented in Fig. 6. In statics, the threshold strain at which permeability starts to grow corresponds to the onset of damage. In dynamics, the rate dependent response of the material enters in the dynamic damaging process. The order of magnitude of the strain rate in the present dynamic tests can be estimated from the pressure profile in Fig. 4-a. The maximum pressure of 3 MPa is reached in about 1 μs. Considering that the dynamics modulus of the mortar is about 20 000 MPa (a 20% increase compared to statics), the strain rate is $1.5\ 10^{2}\ \mathrm{s}^{-1}$. For a pressure wave with a larger amplitude such as those impacting the mortar specimens (e.g. which has been less attenuated during the propagation in water), the applied strain rate may be higher. If the order of magnitude of the pressure wave increases, a reasonable estimate of the strain rate shows a similar increase of order of magnitude because the time rise of the pressure wave is almost constant [17]. According to the bibliographical synthesis performed by Bishop and Perry [2], the material strength is multiplied at least by 4 for dynamic loads with this range of strain rate (between $10^{2}$ and $10^{3}\ \mathrm{s}^{-1}$). In dynamics, the permeability starts to increase for pressures higher than 90 MPa. Assuming that this value is close to the material apparent strength (same as in statics), it corresponds to an equivalent static strength divided by 4 approximately, close to the static strength of 20 MPa provided in Table 1. Same as in statics, the onset of growth of permeability in dynamics is close to the apparent material strength.

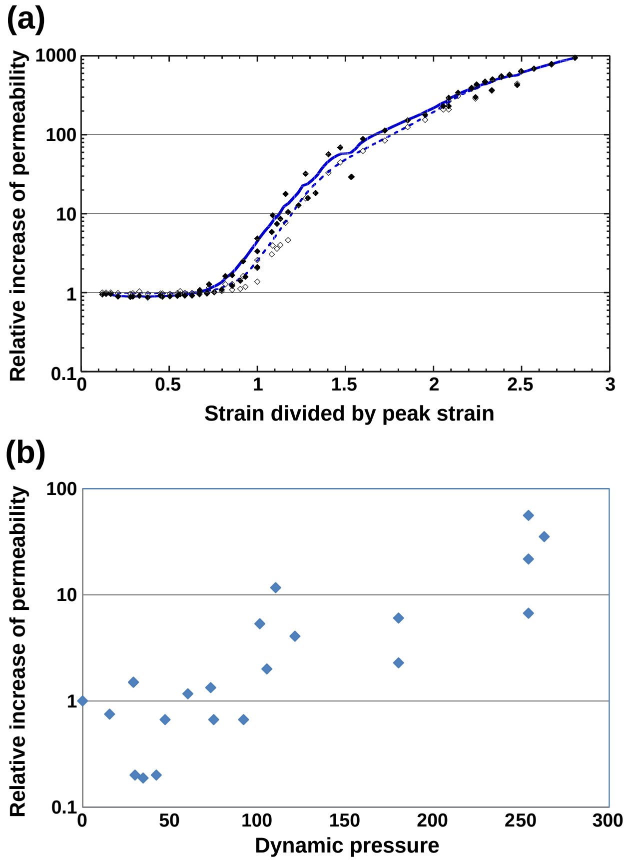

**Fig. 6.** Typical relative evolution of the permeability with applied strain in statics (a) and with pressure in dynamics (b). The results in statics are due to Choinska et al. [5].

The permeability has grown by two orders of magnitude in dynamics for a pressure of 250 MPa. In statics, the same growth is obtained for an applied strain equal to 1.5 the strain at peak load. It is difficult, however, to compare the two evolutions because the state of damage develops in dynamics in a different way compared to statics. It is homogeneous in statics while damage (and permeability) decreases as the wave propagate inside the specimen in dynamics as we will see on X-Ray scans.

### 3.2. Influence of shock number on permeability

The peak pressure value is now set constant, equal to 90 MPa, and the number of shocks applied on the same specimen increases from one to ten (1, 3, 6, 8, 10 shocks). The test results are plotted in Fig. 7. The permeability increases with the number of shocks. This increase spans over an order of magnitude which is above the scattering of data. In a semi-log plot, this increase may be regarded as a linear function in a first approach. Above 8 shocks, some specimens exhibited macrocracks in half of the tested set and it was not possible to measure the overall permeability. The data point for 10 shocks is probably an under estimation of the average permeability (since it is much higher when the specimen is cracked). We could not observe noticeable differences in the values of permeability between the specimens stored in water and the specimens kept under dry conditions. Both sets are plotted in the figure. It should be mentioned however that in spite of the different conservation processes, the specimens have probably not been placed in a sufficiently dry environment for a long enough period of time so that a difference can be noticed.

### 3.3. Evolution of the microstructure illustrated by X-ray scans

X-ray tomography has been used in order to visualize qualitatively the correlations between the mechanical loads, the microstructure of the material and the permeability. In the CT scans, there is a linear relationship between the level of grey and the material density on these images. White zones in Fig. 8 characterize damage in concrete, cracks and micro-cracks where the density is close to zero whereas darkest zones characterise the virgin material with real density close to $2.5\ \mathrm{kg/m}^{3}$.

Fig. 8 shows the effect of shocks of amplitude equal to 250 MPa on the distribution of density (due to micro-cracking). The permeability which is initially in the range of $4 \cdot 10^{-17}\ \mathrm{m}^{2}$ has increased significantly. Recall that the permeability is averaged over a slice of which is 50 mm thick cut from the top of the specimen. On these images, the thickness of the slice corresponds to the radius of the specimen. The window over which the permeability is averaged is

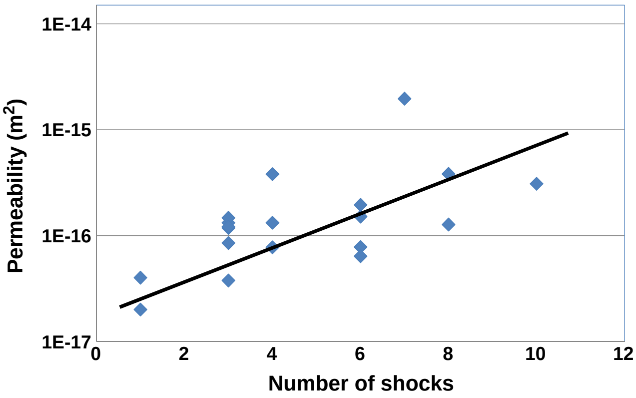

**Fig. 7.** Evolution of the permeability with the number of shocks, under a peak pressure equal to 90 MPa.

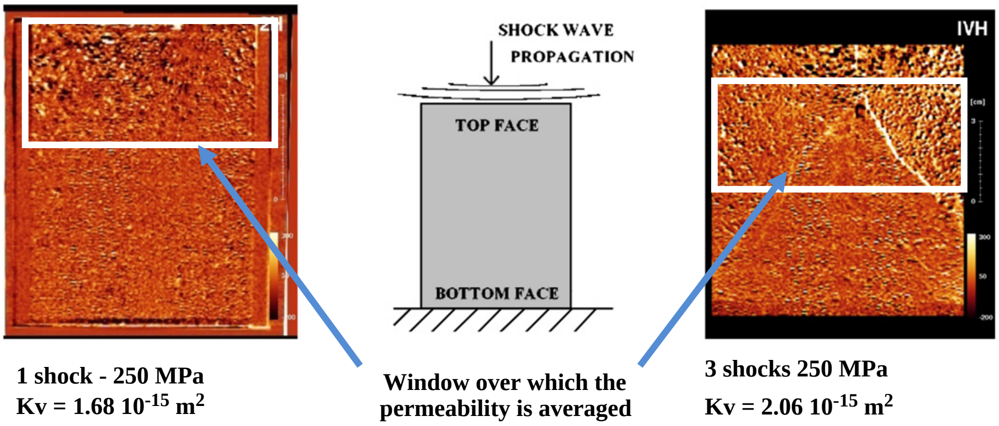

**Fig. 8.** Vertical cross tomography scans after one shock (left) and three shocks (right) under 250 MPa shock wave. The entire specimen has been scanned. The size of the window over which the permeability is averaged is 50 mm by 100 mm.

shown on the figure. An average increase of density is observed, travelling toward the bottom face of the specimen. It is noticeable that in all the scans damage mainly affects the top part of the specimen, directly exposed to the shock wave. Spalling and localised failure is also observed. In the middle and bottom parts of the cylinder, micro-cracking is less noticeable: the effects of the shock wave decreases as the wave propagates through the specimen from the top face to the bottom face. Micro-cracking attenuates the pressure wave (consumption of energy due to cracking) and thus less damage occurs as the pressure wave travels over the specimen toward the bottom face.

After 3 shocks (Fig. 8), severe micro-cracking is observed. On the corresponding scan, localised failure inside the specimen occurred and the surface of the specimen was severely damaged. The permeability could not be measured according to the usual procedure, i.e. from a disk cut from the top face of the specimen because the mortar was too much damaged. The permeability test was performed on a disk of the same thickness (50 mm) extracted 40 mm below the top face.

Fig. 9 shows scans of a specimen which has been subjected to 7 shocks at 90 MPa. The permeability has increased by two orders of magnitude (permeability equal to $1.96 \cdot 10^{-15}$ $m^2$). Repeated shocks of the same amplitude induce an increase of permeability which is the result of the micro-cracking observed on the left scan in Fig. 9. This specimen has been cored and a micro-scan analysis has been carried out with 3D reconstruction of the image. The comparison between scans and micro-scans was performed in order to check that the image analysis (subtraction of two images) on the CT scans did not induce some bias. Fig. 9 (right) shows a cross section of the cored plugs after reconstruction. The resolution is 4 µm. A large number of micro-cracks can be observed in this scan, same as in the CT scan images. These micro-cracks have an opening in the micrometer range, close to the image resolution. They are quite well distributed over the cross section of the plug. It can be noticed that large micro-cracks with a wide opening (e.g. in the range of 100 µm) are not observed. All these observations are going to be quantified in the next section with the help of mercury intrusion porosimetry.

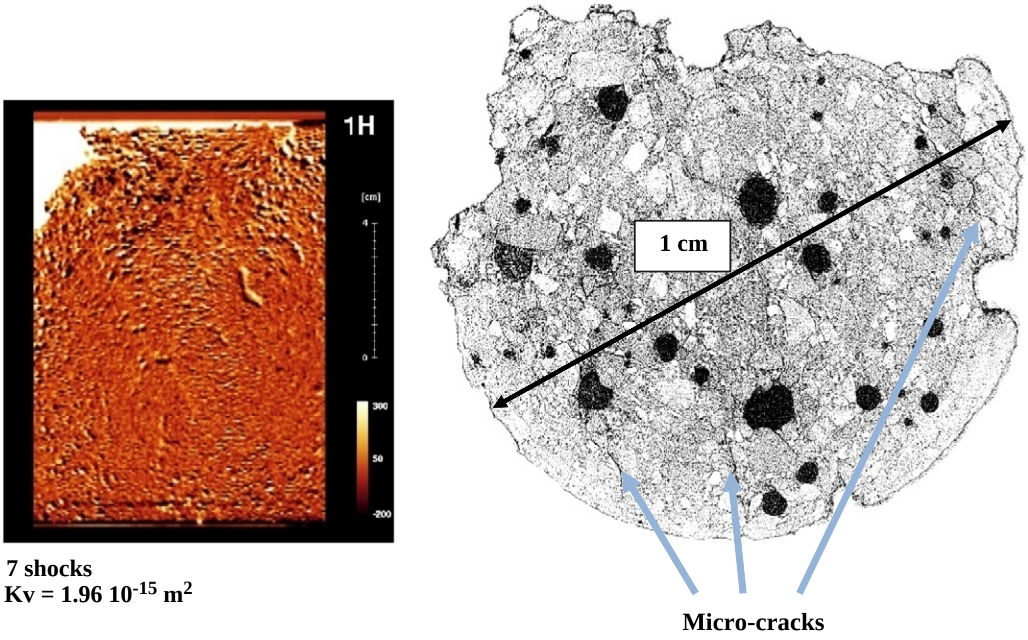

**Fig. 9.** Left: vertical cross tomography scan of entire specimen 1H subjected to 7 shocks at 90 MPa. Right: microscan of a cylindrical plug of diameter 1 cm cored at the surface of the specimen exposed to the shock wave (resolution = 4 µm), inversion of the grey scale in order to visualise cracks and voids (in black).

### 3.4. Pore size distributions

The characterization of the pore size distribution of cementitious materials with the help mercury intrusion techniques (MIP) is a routine technique which has many drawbacks. Among these drawbacks, one can mention that only the porosity accessible from the outer surface is characterised, that the analysis is based on the Washburn equation, with the assumption that pores are cylindrical, or that the “ink bottle effect” is not considered. Diamond [7] reviewed these drawbacks thoroughly, compared data with image analysis techniques, and concluded that MIP underestimated most of the pore size distribution and that it should not be used except for comparison purposes. He concluded that the threshold diameter and intrusion volume could still be useful indexes in comparative studies. We are going here to use this technique in order to compare the same material before and after the shocks. Except for very small pore diameters where the mercury injection pressure induces most certainly a damage of the microstructure of the material and data should not be considered to be representative, we shall assume that all the measurements suffer from the same bias and therefore their comparisons remain meaningful (but not the intrinsic distribution for each microstructure).

Fig. 10 shows the results obtained on three samples cored from the same specimen. The pore size distributions (here fluid intrusion volume per pore of a given size) are quite similar. Considering this result, average distributions will be used in further comparisons. Table 2 presents the global measurements of mercury intrusion porosity as a function of the number of shocks. The measures have been made on three samples cored from each specimen tested except in case of seven shocks because the mortar was so damaged that it was possible to drill one single core only. For the samples tested, the total intrudable pore volume is almost constant with the number of shocks applied to the specimen. There is a slight decrease which is within the scattering of data. The average pore diameter increases with the number of shocks. The pore size distribution seems to change but the intrudable volume is constant.

Fig. 11 shows the evolution of average pore size distributions for the specimens subjected to repeated shock waves of maximum amplitude equal to 90 MPa. For the sound mortar, the maximum intrusion volume is found for a pressure corresponding to a diameter of 0.1 μm. The curve of pore size distribution is characteristic of a bimodal, gauss type, distribution with two peaks for pore sizes of 0.1 μm and 1 μm.

The distributions for damaged samples are quite different: the intrusion volume in pores with 0.1 μm diameter decreases with increasing number of shocks whereas it increases for pores of sizes between 5 μm and 15 μm approximately. Above this size, there are no significant differences and the pore size distributions do not seem to be affected by the shock waves. There are respectively, two maxima at 0.1 μm and 2 μm for three shocks damaged samples and two maxima for 0.1 μm and 7 μm for seven shocks damaged samples. Mortar damaged with seven shocks contains more micro-pores with radius greater than 7 μm than the mortar damaged with three shocks. The void size distribution of the specimen subjected to seven shocks exhibits a third maximum for small pore diameters ranging from 0.01 μm to 0.06 μm. This result is not representative because the MIP technique is not appropriate in this range of pore diameter.

**Table 2**
Results from mercury intrusion porosimetry.

| Samples | Porosity (intrudable pore volume) (%) | Average pore diameter (μm) | Real density ($g/cm^3$) | Apparent density($g/cm^3$) |
|---|---|---|---|---|
| 0 shocks | 23.32 | 0.13 | 2.51 | 1.92 |
| 3 shocks | 23.16 | 0.15 | 2.48 | 1.92 |
| 7 shocks | 23.03 | 0.19 | 2.57 | 1.97 |

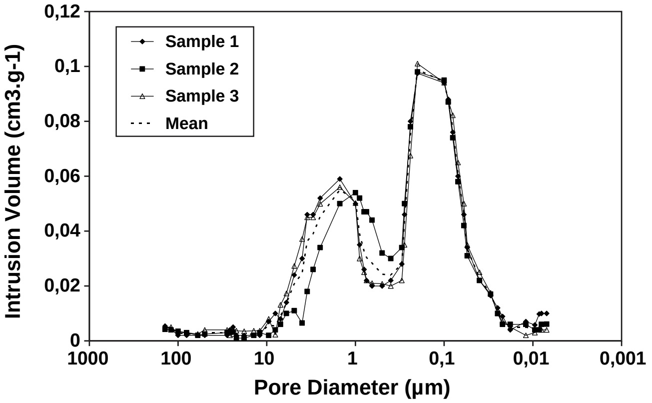

**Fig. 10.** Comparison between the pore size distributions of three samples from the same specimen.

We may conclude that the volume of pores of initially sub-micrometric sizes (as measured by MIP) decreases and the volume of pores of micro-metric size (as measured by MIP) is increasing as the number of shock increases. Two processes may be considered: the closure of pores due to the compressive pressure wave and the opening of pores to the extensions involved in the compressive loading. Some pores of sub-micrometric size are being closed and some are growing in size, the processes are mixed and modifications of the connectivity of the porous network may also occur. Overall, pores of sub-micrometric size probably evolve and become larger. What is rather unexpected is that pores of large diameter (above 50 μm) do not evolve. We shall conclude that the micro-structural damage process starts at the sub-micrometric scale and seems to evolve towards larger characteristic scales.

## 4. Conclusions

This paper deals with the experimental correlation between the response of mortar submitted to dynamic loads and its mass transfer properties. It investigates the influence of the applied maximal pressure and of the number of applied shock waves on the permeability to gas of mortar specimens and the evolution of their microstructure (pore size distribution and micro-cracks).

The dynamic load is applied to the mortar using shock waves generated by a subsonic discharge between two electrodes in water. It is possible to control the amplitude of the pressure wave depending on the electrical energy that is stored in capacities prior to electrical breakdown.

Results from single shock tests show that there is a threshold of maximum amplitude of the shock wave above which damage is

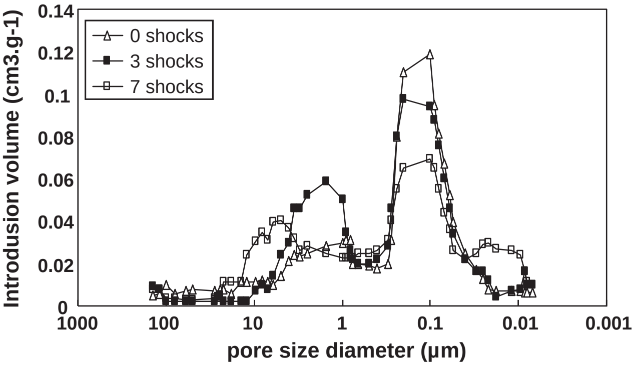

**Fig. 11.** Effect of number of shocks (amplitude 90 MPa) on the pore size distribution.

observed. The evolution of the permeability is qualitatively the same as in statics, with different stress levels due to dynamic effects. Tests with repeated shocks, even with a moderate amplitude corresponding to the threshold observed for single shock tests, show that there is an accumulation of damage as a function of the number of shocks. An increase of permeability is also observed. This phenomenon remains to be thoroughly explained, for instance damage deactivation due to micro-crack closure could allow this accumulation of damage.

Qualitative results of image analysis (X Ray Tomography) illustrate the evolution of the microstructure of the material leading to the increase of permeability. Diffuse microcracking is observed prior to specimen failure, with a significant increase of permeability. Comparative results from mercury intrusion porosimetry (MIP) show that the micro-structural damage process starts at the sub-micrometric level and that the characteristic size of pores of growing volume increases. The theoretical correlation between the pore size distribution and the frequency content of the pressure wave has to be further investigated.

## Acknowledgements

Financial support from Total SA within the TGR project is gratefully acknowledged. The authors would like also to thank Total SA for providing the access to the scanning facility and for having performed the image analyses.

## References

[1] A. Beroual, M. Zahn, A. Badent, K. Kist, A.J. Schwabe, H. Yamashita, K. Yamazawa, M. Danikas, W.G. Chadband, Propagation and structure of streamers in liquid dielectrics, IEEE Electrical Insulation Magazine 14 (2) (1998) 6–17.
[2] P.H. Bishop, S.H. Perry, Compressive behaviour of concrete at high strain rates, Materials and Structures 24 (1991) 425–450.
[3] J. Cao, D.D.L. Chung, Defect dynamics and damage of concrete under repeated compression, studied by electrical resistance measurement, Cement and Concrete Research 31 (2001) 1639–1642.
[4] J. Cao, D.D.L. Chung, Minor damage of cement mortar during cyclic compression, monitored by electrical resistivity measurement, Cement and Concrete Research 32 (2001) 1656–1662.
[5] M. Choinska, A. Khelidj, G. Chatzigeorgiou, G. Pijaudier-Cabot, Effects and interactions of temperature and stress-level related damage on permeability of concrete, Cement and Concrete Research 37 (2007) 79–88.
[6] C. Denoual, F. Hild, Dynamic fragmentation of brittle solids: a multi-scale model, European Journal of Mechanics, A/Solids 21 (2002) 105–120.
[7] S. Diamond, Mercury porosimetry – an inappropriate method for the measurement of pore size distributions in cement-based materials, Cement and Concrete Research 30 (2000) 1517–1525.
[8] A. Ginenko, V. Gurovich, Y. Krasik, A. Sayapin, S. Efimov, J. Felsteiner, Analysis of shock wave measurements in water by a piezoelectric pressure probe, The Review of Scientific Instruments 75 (1) (2004) 240–244.
[9] N. Hearn, B. Lok, Measurement of permeability under uniaxial compression: a test method, American Concrete Institute Materials Journal 95 (6) (1998) 691–694.
[10] S. Katsuki, H. Akiyama, A. Abou-Ghazala, K.H. Schoenbach, Parallel streamer discharges between wire and plane electrodes in water, IEEE Transactions on Dielectrics and Electrical Insulation 9 (4) (2002) 498–506.
[11] A. Kermani, Permeability of stressed concrete, Building Research and Information 19 (6) (1991) 360–366.
[12] I.V. Lisitsyn, H. Nomiyama, S. Katsuki, H. Akiyama, Thermal processes in a streamer discharge in water, IEEE Transactions on Dielectrics and Electrical Insulation 6 (4) (1999) 351–356.
[13] L.J. Klinkenberg, The permeability of porous media to liquid and gases, Drilling and production practice, American Petroleum Institute, 1941, pp. 200–213.
[14] M. Matallah, *Les ondes de chocs,* Internal report, LASAGEC$^2$, Tight gas project, Université de Pau et des Pays de l'Adour, Anglet, France, 26 pages, 2008.
[15] H. Meziani, F. Skoczylas, An experimental study of the mechanical behaviour of a mortar and of its permeability under deviatoric loading, Materials and Structures 32 (1999) 403–409.
[16] V. Picandet, A. Khelidj, G. Bastian, Effect of axial compressive damage on gas permeability of ordinary and high-performance concrete, Cement and Concrete Research 31 (2001) 1525–1532.
[17] G. Touya, T. Reess, L. Pécastaing, A. Gibert, P. Domens, Development of subsonic electrical discharges in water and measurements of the associated pressure waves, Journal de Physique D: Applied Physics 39 (2006) 5236–5244.